Barium titanate ground- and excited-state properties from first-principles calculations

S. Sanna,[1,*] C. Thierfelder,[1] S. Wippermann,[1] T. P. Sinha,[2] and W. G. Schmidt[1]
[1]*Lehrstuhl für Theoretische Physik, Universität Paderborn, D-33095 Paderborn, Germany*
[2]*Department of Physics, Bose Institute, Kolkata 700009, India*
(Received 21 September 2010; revised manuscript received 7 January 2011; published 23 February 2011)

We present a comprehensive theoretical investigation of paraelectric (cubic) and ferroelectric (tetragonal) $BaTiO_3$. The atomic and electronic structure, piezoelectric tensor, Debye temperature, zone center phonon frequencies, and optical absorption are calculated for both phases from first principles. The structural and vibrational properties predicted from density functional theory are in good agreement with experiment and earlier theoretical work. The electronic structure and optical response are found to be very sensitive to quasiparticle and electron-hole attraction effects, which are accounted for by using the GW approach and by solving the Bethe-Salpeter equation, respectively. Electronic self-energy effects are found to open the band gap substantially, to 3.7 and 3.9 eV for the cubic and tetragonal phases, respectively. In contrast to earlier calculations, good agreement with the measured optical data is achieved. The *ab initio* thermodynamics predicts that the ferroelectric ordering will disappear at 419 K. It is shown that the phase transition is driven by the vibrational entropy of a variety of modes.

DOI: 10.1103/PhysRevB.83.054112 PACS number(s): 77.84.Cg, 71.15.Mb, 78.20.Bh, 61.50.Ah

I. INTRODUCTION

Barium titanate ($BaTiO_3$, BT) is a synthetic material that crystallizes either in the perovskite crystal structure[1–3] or in its hexagonal modification (h-$BaTiO_3$).[4,5] The perovskite polymorph undergoes a sequence of ferroelectric transitions with growing temperature. At 183 K, the structure transforms from rhombohedral to orthorhombic and the polarization direction changes from the [111] to the [110] direction. At 278 K, the structure becomes tetragonal, with spontaneous polarization directed along the [100] direction. Finally, at 393 K, $BaTiO_3$ assumes a cubic symmetry with no net polarization. Because of the number of different ferroelectric phases and the ease of switching back and forth between them, BT is both of great scientific interest and technological relevance. Indeed, it is the prototypical ferroelectric oxide, as many features and properties caused by or related to ferroelectricity have been found for the first time in BT. The technological relevance is due to the still growing employment of BT for various technical applications in fields such as electronics, electromechanical energy conversion, nonlinear optics, and nonvolatile data storage.[6] Previous experimental and theoretical studies have focused on the structural, elastic, thermal,[1,2,7,8] electronic,[9–11] optical,[9,10] and vibrational[12,13] properties of the different phases. Furthermore, electron-spin resonance[14] as well as X-ray diffractometry[15] have been used to determine the dominant intrinsic defects in BT bulk and the structural properties of $BaTiO_3$ nanocrystalline powders. Early theoretical investigations (see for example Refs. 16 and 17 and references therein) date back to the 1960s. In the past 20 years, several first-principles calculations on BT have been performed that address the structural, mechanical, and electronic properties of the four phases[3,18–20] and the origin of the ferroelectricity.[21] The phonon dispersion has been calculated for the cubic phase,[22] and the optical properties (at different levels of approximation) for the cubic and tetragonal phases.[23–26] However, none of the exchange-correlation potentials commonly used within the density functional theory (DFT)[27,28] is able to provide at the same time an accurate description of both the electronic and the structural properties of BT.[29–32] Neither the standard local density approximation (LDA)[33] and generalized gradient approximation (GGA)[34] nor the hybrid functionals[35–37] are sufficiently accurate for a complete description of the four phases. Most local functionals predict the BT structure with an acceptable precision but underestimate the electronic band gap, while hybrid functionals yield an improved band gap but overestimate the lattice constant and the atomic distortion associated with the ferroelectricity. This is particularly problematic in the study of ferroelectric oxides, as the structural instabilities that give rise to the ferroelectricity are highly sensitive to volume changes and strongly linked to the electronic states at the valence band maximum (VBM) and conduction band minimum (CBM). The theoretical description of the optical properties is not satisfactory either, as the calculated adsorption peaks are either redshifted[25] or have a wrong line shape[19] in comparison with the measured spectra. Most theoretical investigations of BT deal with the highly symmetric cubic phase, while the tetragonal phase, stable at room temperature, is far less investigated. The ferroelectric phase transition is also still an object of investigation.[22] Its study (both experimental and theoretical) is made difficult by the small size of the atomic displacements and energy differences. For this reason impurities, point and extended defects, stress, and even light can affect the transition. Cohen and Krakauer[18] and later Wahl *et al.*[32] and Xie *et al.*[22] calculated the lowest frequency F_{1u} phonon mode, related to the structural distortions in the ferroelectric phase, as a function of the crystal volume. They found that the ferroelectric instability arises largely from the covalent hybridization between the Ti and the O ions.

In this work we present the results of our first-principles investigation of thermal, electronic, and optic excitations of high-temperature (cubic) and room-temperature (tetragonal) BT. Structural and vibrational properties are calculated in the framework of the DFT-GGA (the PW91 formulation).[38] In order to address the discrepancies between measured and

 ©2011 American Physical Society

calculated excitation properties, we calculate the electronic and optical properties, accounting for quasiparticle effects within the GW approach[39] and for electron-hole attraction[40–42] by solving the Bethe-Salpeter equation (BSE).[43–45] The ferroelectric phase transition is investigated by means of first-principles thermodynamics. The paper is organized as follows: After a brief introduction to the computational scheme (Sec. II), we determine the structurally relaxed ground state of both the ferro- and paraelectric BT phases. The reliability of our scheme is demonstrated by comparing the structural and vibrational properties with earlier theoretical data and experiment. Then, the electronic quasiparticle spectrum is obtained within the GW approximation (GWA) to the exchange-correlation self-energy, using the DFT-GGA Kohn-Sham eigenvalues and eigenfunctions that enter the single- and two-particle Green's functions. Finally the Bethe-Salpeter equation is solved for coupled electron-hole excitations, thereby accounting for the screened electron-hole attraction and the unscreened electron-hole exchange (Sec. III). In Sec. IV we discuss the ferroelectric phase transitions, and in Sec. V we summarize the main results of this work.

II. METHODOLOGY

Our first-principles calculations within the density functional theory (DFT) use the projector augmented wave method[46] (PAW) as implemented in VASP.[47] The PW91 formulation of the generalized gradient approximation (GGA) exchange-correlation (XC) functional,[38,48] plane wave expansions up to 550 eV, and projectors up to $l = 3$ for Ti and $l = 2$ for Ba and O have been used for the calculations. The $5s$ electrons of Ba ([Xe] $5p6s$) are treated as valence states. King-Smith and Vanderbilt[49] have pointed out that the low-frequency phonon modes related to the ferroelectric instability of many perovskite compounds including BT are remarkably sensitive to the k-point sampling and that rather dense meshes are needed for an accurate description. Therefore, even if the total energies are already converged up to 1 meV with a regular $8 \times 8 \times 8$ Monkhorst-Pack[50] k-point mesh, a shifted $12 \times 12 \times 12$ Monkhorst-Pack (1728 irreducible points) mesh is used for the Brillouin zone integrations. This allows us to calculate the low-frequency phonon modes with an uncertainty of 0.1 cm^{-1}. The BSE calculations were carried out using a mesh of 728 irreducible k points. With this choice we obtain converged spectra.

The electronic self-energy effects are included by replacing the GGA exchange and correlation potential with the nonlocal and energy-dependent self-energy operator $\Sigma(\mathbf{r},\mathbf{r}';E)$. We thereby calculate Σ in the GW approximation,[39] from the convolution of the single-particle propagator G and the dynamically screened Coulomb interaction W. The screening is calculated in the independent-particle approximation. To take into account the electron-hole interaction, we consider the two-particle Hamiltonian

$$\begin{aligned} H_{vc\mathbf{k},v'c'\mathbf{k}'} &= (\epsilon_{c\mathbf{k}} - \epsilon_{v\mathbf{k}})\delta_{vv'}\delta_{cc'}\delta_{\mathbf{k},\mathbf{k}'} \\ &+ 2\int\int d\mathbf{r}\,d\mathbf{r}'\psi^*_{c\mathbf{k}}(\mathbf{r})\psi_{v\mathbf{k}}(\mathbf{r})\bar{v}(\mathbf{r}-\mathbf{r}')\psi_{c'\mathbf{k}'}(\mathbf{r}')\psi^*_{v'\mathbf{k}'}(\mathbf{r}') \\ &- \int\int d\mathbf{r}\,d\mathbf{r}'\psi^*_{c\mathbf{k}}(\mathbf{r})\psi_{c'\mathbf{k}'}(\mathbf{r})W(\mathbf{r},\mathbf{r}')\psi_{v\mathbf{k}}(\mathbf{r}')\psi^*_{v'\mathbf{k}'}(\mathbf{r}'), \end{aligned} \tag{1}$$

which describes the interaction of pairs of electrons in conduction states $|c\mathbf{k}\rangle$ and holes in valence states $|v\mathbf{k}\rangle$.[43–45] The first (diagonal) term contains the quasiparticle energies from the GW approximation. The second term is the electron-hole exchange term; it contains the short-range part of the bare Coulomb potential $\bar{v}$ and represents the effect of local fields. The third part describes the screened electron-hole attraction and is calculated using a model dielectric function.[51] In this approximation, the wave-vector ($\mathbf{q}$) dependence of the dielectric function is given by

$$\epsilon(\mathbf{q},\rho) = 1 + \left[\frac{1}{\epsilon_\infty - 1} + \left(\frac{q}{q_{TF}(\rho)}\right)^2 + \frac{3q^4}{4k_F^2(\rho)q_{TF}^2(\rho)}\right]^{-1}, \tag{2}$$

where k_F and q_{TF} represent the Fermi and Thomas-Fermi wave vectors, respectively, which depend on the electron density ρ. This expression interpolates between the correct behaviors at high and low $\mathbf{q}$ vectors and, by construction, correctly obtains the static dielectric constant for $\mathbf{q} = 0$. For the actual calculation of the polarizability, we use the time-evolution implementation described in Refs. 52 and 53.

The ferroelectric phase transition is investigated by means of *ab initio* thermodynamics. The ground state of $BaTiO_3$ at a given pressure p and temperature T is characterized by the lowest Gibbs free energy:

$$G(p,T) = U + pV - TS, \tag{3}$$

where U is the internal energy of the system and S its entropy.[54] For zero pressure, the Gibbs free energy G coincides with the free energy $F = U - TS$. For a solid, with no rotational and translational degrees of freedom, it can be decomposed in an adiabatic approximation to an electronic and a vibrational contribution:

$$F = F^{\mathrm{el}} + F^{\mathrm{v}}. \tag{4}$$

As the considered BT phases are characterized by a noticeable electronic band gap (i.e., $\approx$2 eV), the electronic contributions to the entropy can be considered vanishing. Therefore, the dominant term is

$$F^{\mathrm{v}} = \frac{\Omega}{8\pi^3}\int d^3\mathbf{k}\sum_j \frac{1}{2}\hbar\omega_j(\mathbf{k}) + k_BT\ln\left(1 - e^{-\frac{\hbar\omega_j(\mathbf{k})}{k_BT}}\right), \tag{5}$$

where $\omega_j(\mathbf{k})$ is the wave-vector-dependent frequency of the jth phonon branch. We note here that the frequencies and the corresponding eigenvectors are calculated within the harmonic approximation from the force-constant matrix. This, in turn, is calculated approximating the electronic free energy of the system $F(V,T)$ with the DFT total energy $E^{\mathrm{tot}}(T = 0)$. (See Refs. 54 and 55.)

III. RESULTS

A. Lattice Parameters

The calculated lattice parameters of BT in the high-temperature cubic phase and in the room-temperature tetragonal phase are reported in Table I. Our PW91 calculations overestimate the measured values by 0.8% for the lattice

TABLE I. $BaTiO_3$ calculated and measured lattice parameters (in Å). δ(Ti), $\delta(O_\parallel)$, and $\delta(O_\perp)$ are the atomic displacements parallel to the z axis of the Ti and of the two inequivalent oxygen sites in fractions of the lattice constant c. The results of previous DFT-PBE calculations are reported for comparison.

	PW91	PBE[32]	Exp.[2,56]
		Cubic	
a	4.032	4.035	4.00
		Tetragonal	
a	4.005	4.005	3.986
c/a	1.048	1.050	1.010
δ(Ti)	0.019	0.018	0.015
$\delta(O_\parallel)$	−0.025	−0.027	−0.014
$\delta(O_\perp)$	−0.045	−0.047	−0.023

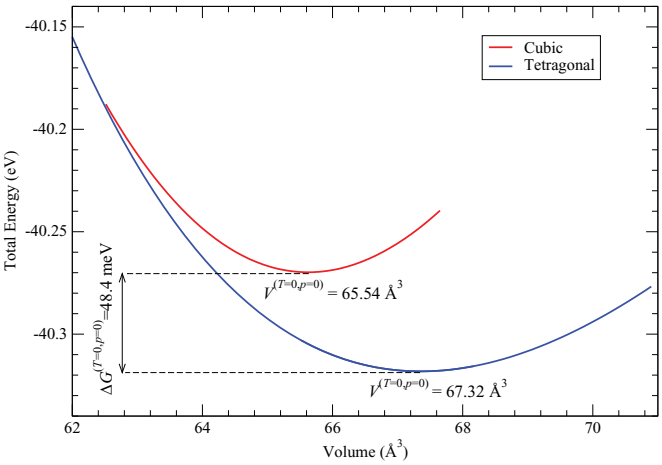

FIG. 1. (Color online) Total energy as a function of the volume for the cubic and tetragonal unit cells of $BaTiO_3$. The energy difference between the two minima represents the Gibbs energy difference $\Delta G(T = 0, p = 0)$ of the two phases at zero temperature and pressure.

constant of the cubic phase and by 0.5% and 4.2% for the a and c parameters of the tetragonal phase, respectively. The deviations from the experimental values are similar to previous calculations[29,31,32] and affected by the well-known overtetragonality problems (overestimation of the c/a ratio) in the description of the ferroelectric phase.[31] The calculated energy difference between the two phases, $\Delta E = 48.4$ meV per formula unit, is similar in magnitude to that found with DFT-PBE simulations in Ref. 31 (49.3 meV). Even if the accuracy of a DFT calculation is considered to be of the order of 1 meV, energy differences between different phases may be more accurate, since a considerable error cancellation occurs in the calculation of the total energy of two supercells containing the same atoms and carried out with the very same numerical parameters. The bulk modulus B and its first pressure derivative B' have been derived by fitting the energy-volume curves (calculated at $T = 0$ K) to the Murnaghan equation (see Fig. 1). The calculated values ($B = 163.0$ GPa, $B' = 4.5$ for the cubic phase and $B = 85.6$ GPa, $B' = 10.9$ for the tetragonal phase) are in excellent agreement with the available experimental data.[56]

The relaxed-ion piezoelectric stress tensor e_{ijk} has been calculated using density functional perturbation theory as described in Refs. 57–59. Our approach takes into account the contributions from the lattice relaxation.[60] The piezoelectric strain tensor d_{ijk} is then derived by solving the tensor equation

$$e_{ijk} = c_{lmjk} d_{ilm}, \tag{6}$$

where c_{lmjk} are the elastic constants calculated at constant electric field. The number of indices can be reduced by introducing the matrix (or Voigt) notation. The relationship between tensor indices and matrix indices is given by

$$\begin{array}{lcccccc} \text{Tensor} & 11 & 22 & 33 & 23,32 & 31,13 & 12,21 \\ \text{Matrix} & 1 & 2 & 3 & 4 & 5 & 6. \end{array} \tag{7}$$

Although the relationship between the indices of the tensor components and matrix elements is unambiguous, it is defined to the extent of a multiplication factor. The elements (d_{in}) of the piezoelectric matrix are formed from the $[d_{ijk}]$ tensor components with the following summation convention:

$$\begin{cases} d_{in} = d_{ijk} & \text{if} \quad n = 1,2,3 \\ d_{in} = 2d_{ijk} & \text{if} \quad n = 4,5,6. \end{cases} \tag{8}$$

The total number of independent tensor components is determined by the point group of the material. This leads for tetragonal $BaTiO_3$ with point group $4mm$ to three independent tensor elements, in Voigt notation d_{31}, d_{33}, and d_{15}, often called *piezoelectric constants*. The calculated tensor components are given in Table II, where the measured values are reported for comparison. Our calculations correctly reproduce the sign and the magnitude of the measured tensor components.[61,62] The quantitative agreement is poor, however. In particular, d_{15} is underestimated. The deviation from the experiment results from the simultaneous overestimation of c_{55} and underestimation of e_{15}. However, the comparison of calculated and measured tensor components is made difficult by the uncertainties and systematic errors affecting the measurements, and by the sensitivity of the calculations.[63] Indeed, small errors in the calculation of the elastic constants or dipole moments may have a large influence on the calculation of the piezoelectric tensor. With the calculated elastic constants it is possible to estimate the Debye temperature ϑ_D of the material. Siethoff and Ahlborn[64] have shown that the relationship between ϑ_D and elastic constants is given, for tetragonal crystals, by

$$\vartheta_D = \frac{C_B h}{k_B \sqrt[6]{s}} \sqrt{\frac{a G_T}{M}}, \tag{9}$$

where C_B is a constant equal to 5.05×10^{11} obtained by fitting all the analyzed tetragonal materials to Eq. (9). Here h and k_B are the Planck and Boltzmann constants, s and M are the number of atoms and the weighted average of the

TABLE II. Relaxed-ion piezoelectric tensor components d_{ij} (10^{-11} C/N) for tetragonal $BaTiO_3$.

Component	Theory	Exp.
d_{31}	−1.48	−3.34
d_{33}	9.02	9.00
d_{15}	1.00	28.20

atomic masses in the crystallographic unit cell, a is the lattice parameter, and

$$G_T = \left[\frac{(c_{11} - c_{12})c_{44}c_{66}}{2}\right]^{\frac{1}{3}} \quad (10)$$

gives the proportionality to the lattice constants (here expressed in Voigt notation). With the calculated lattice parameter and c_{ij} we obtain a Debye temperature $\vartheta_D = 513$ K, which is a good estimate of the measured value (480.16 K) reported in Ref. 63.

The relaxed ground-state geometries for ferroelectric and paraelectric BT are used as the starting point for all further investigations.

B. Vibrational properties and ferroelectric instability

The calculated frequencies of the Γ-phonon modes of the cubic phase, which can be compared to previous calculations and experiment, are given here to allow an assessment of the accuracy of our approach. The phonon modes of the tetragonal phase had not been calculated before and are reported for the first time. Furthermore, we use this section to briefly discuss the ferroelectric instability, which is strongly connected with the vibration modes. The lattice dynamics of the different $BaTiO_3$ phases were investigated experimentally in the 1970s in order to explain the mechanisms of the (ferroelectric) phase transition.[13] Since then, starting with the work of Cohen and Krakauer[18] different theoretical investigations of the BT vibrational properties have appeared. Tinte *et al.*[29] as well as, more recently, Wahl *et al.*[32] and Bilc *et al.*[31] have calculated the phonon modes of cubic $BaTiO_3$ within different approaches. These investigations have shown that the phonon frequencies of the cubic phase do not *directly* depend on the exchange-correlation potential but are quite sensitive to the cell volume, which in turn strongly depends on the XC potential. As first noted by Cohen,[18] the c/a lattice strain at fixed volume increases the Ti-O distance along the tetragonal axis, thus facilitating the [001] ferroelectric distortion. In particular, an underestimation of the crystal volume leads to the inhibition of the modes responsible for the ferroelectric instability. This is consistent with the experimental observation that BT loses ferroelectricity at high pressures.[65] We perform our calculation at the calculated volume. The phonon modes and frequencies are calculated using the frozen-phonon approach.[66]This approach does not include the long-range electric fields that accompany longitudinal phonons. For this reason, we restrict ourselves to the transverse modes. All the modes are calculated with fully relaxed geometries. The unit cell of $BaTiO_3$ contains five atoms, which yields (excluding the translational modes) 12 phonon modes. The cubic phase exhibits four triply degenerate distinct modes, which split into a doublet (E mode) and a singulet (A_1 mode) each in the tetragonal phase. At the Γ point, the optical phonons can be classified according to the irreducible representations of the space group $Pm\bar{3}m$ into three Γ_{15} modes with F_{1u} symmetry and one Γ_{25} mode with F_{2u} symmetry. In Table III we assign our results to the experimental findings for the respective modes. The modes belonging to the first optical branch (TO1) have imaginary frequencies, as they represent a saddle point of the total energy. Within deviations of at most 18 cm^{-1}, the calculated frequencies match the experimental results and, in the case of cubic BT, are similar to previous calculations.[32] To our knowledge, our work is the first theoretical investigation that addresses the phonons of the ferroelectric phase and confirms the phonon splitting observed upon the cubic-tetragonal phase transition.[13] The biggest singlet-doublet splitting is observed for TO1, a phonon branch characterized by the relative movement of the oxygen ions with respect to the Ti ion, which has been considered responsible for the ferroelectric instability.[21] This phonon mode, whose dispersion has been calculated by Xie *et al.*,[22] is depicted in Fig. 2(d). The other TO1 phonons are also represented in Fig. 2. The triplet of the cubic phase is split into a singlet and doublet with higher frequencies. This shift in the frequency can be understood by way of the hybridization of the Ti $3d$ with the O $2p$ orbitals suggested by Cohen and Krakauer,[18] which results in larger force constants. In further agreement with the measurements of Ref. 13, we observe the continuity of the three E-type modes in the tetragonal phase correlated with the three F_{1u} modes in the cubic phase. The correct description of the phonon modes is of particular relevance, as the vibrational entropic contribution to the free energy enters into the calculation of the phase transition.

TABLE III. Frequencies (cm^{-1}) of the optical phonons at the center of the Brillouin zone. Phonon modes are calculated at the GGA volume.

Cubic			Tetragonal	
	Calc.	Exp.	Mode	Calc.
F_{1u} (TO1)	198i	soft	A_1	363
			E	122i
F_{1u} (TO2)	178	182	A_1	152
			E	163
F_{1u} (TO3)	466	482	A_1	562
			E	451
F_{2u}	288	306	A_1	275
			E	290

C. Electronic structure

There have been different attempts to calculate the electronic structure of cubic[23,31] and tetragonal[17,19] BT. We note that the band dispersion depends on the XC potential used. While cubic BT seems to be a direct semiconductor at Γ within LDA,[23] GGA and hybrid potentials yield an indirect Γ-R gap.[31] In this work the electronic band structure of cubic and tetragonal BT has been calculated within different approaches. In Fig. 3 (solid lines) we plot the Kohn-Sham

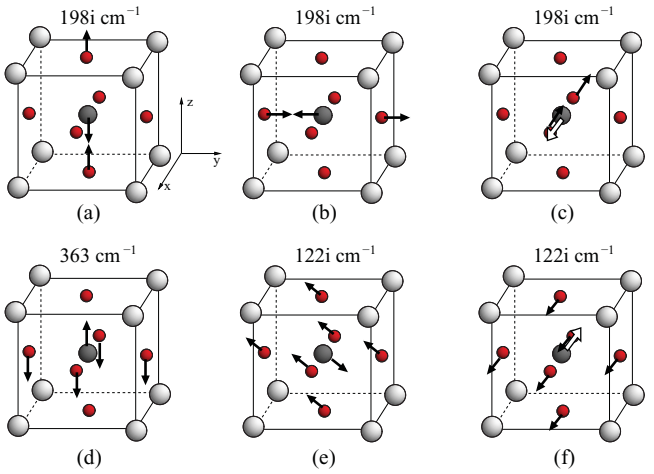

FIG. 2. (Color online) Schematic representation of the eigenvectors of the phonon modes belonging to the first optical branch (TO1) of cubic and tetragonal $BaTiO_3$. The phonon mode of the isotropic cubic phase [(a), (b), and (c)] is triply degenerate and represents the reciprocal movement of one oxygen atom and the Ti atom in the three spatial directions. This mode splits in the tetragonal phase into a singlet (d), with oxygen atoms and Ti vibrating in opposite directions along the z axis and originating the ferroelectric instability, and a doublet, with Ti and the O_3 group, vibrating in opposite directions in the nonpolar xy plane [(e), (f)].

energy eigenvalues calculated along the high-symmetry lines of the cubic and tetragonal Brillouin zone shown in Fig. 4. The DFT band gap of 1.63 eV for the paraelectric phase and 1.71 eV for the tetragonal phase is in agreement with previous calculations. Strictly speaking, BT has an indirect band gap (CBM at Γ and VBM at R in the cubic and A in the tetragonal phase). However, the uppermost valence band is relatively flat, so that BT can be approximatively regarded as a direct semiconductor at Γ in both cases. The valence band, with a band width of about 5 eV, is mainly derived from O $2p$ states, while the lowest part of the conduction band has mainly Ti $3d$ character. The lowest valence bands visible in Fig. 3, located 10 eV below the VBM, are related to the Ba $5d$ orbitals. While the dispersion of the bands is in reasonable agreement with photoemission measurements,[67] the calculated band gap is well below the measured optical band gap of 3.3 eV (cubic BT).

To go beyond the single-particle approximation we perform GW calculations for both the ferroelectric and paraelectric phases. The correspondingly corrected energy bands are shown with dotted lines in Fig. 3. The energetic positions of the bands change with the inclusion of quasiparticle effects: The Ti $3d$ conduction bands are shifted upward by about 1.8 eV, while the O $2p$ bands are shifted downward by about 0.2 eV and the Ba $5d$ by about 1.6 eV. The effect of the GW calculations on the band dispersions, however, is small, below 0.1 eV. Quasiparticle effects open the BT band gap significantly. The DFT + GW band gaps amount to 3.68 and 3.90 eV for the cubic and tetragonal phases, respectively. This exceeds the measured optical gap of 3.3 eV (cubic BT) and may be related to excitonic effects. In fact, the discrepancy seemingly observed by the calculated quasiparticle gap and

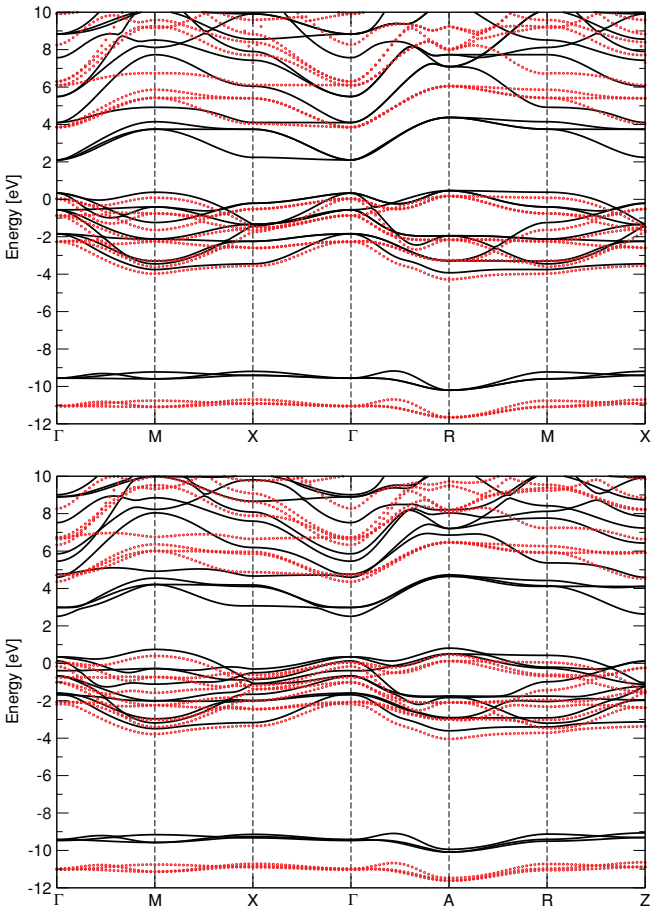

FIG. 3. (Color online) $BaTiO_3$ band structure calculated within the DFT-GGA (solid lines) and the GW approximation (dotted lines) for the paraelectric (top panel) and ferroelectric (bottom panel) phase.

the experimental value corresponds to the excitonic shift at the optical absorption onset, as discussed below.

D. Optical properties

The optical properties of the cubic and tetragonal phase of BT were intensively investigated in the 1960s and 1970s.[9–11] In particular, the optical adsorption spectra were deduced from reflectivity measurements by Kramers-Kronig analysis.[10,11]

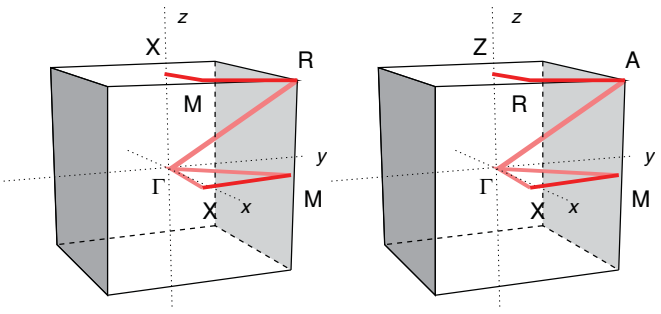

FIG. 4. (Color online) Path joining the high-symmetry points in the Brillouin zone used for the band structure calculation of the cubic (left-hand side) and tetragonal phase (right-hand side) of $BaTiO_3$. The tetragonal distortion occurs along the z axis.

Despite the tetragonal distortion, the optical spectra of the two phases show similar features, which has been traced back to the small effect of tetragonality (10–150 meV) on the band structure.[10,17] Two main adsorption peaks at 4.8 eV (labeled with P_1 in this work) and around 10.5 eV (P_2, with two side peaks P_2' and P_2'' at around 8.2 and 11.7 eV) dominate the spectrum.[11] Smaller features at 6 and 7.3 eV are also observable. The previous theoretical description of these features is not really satisfactory. Saha *et al.*[23] found with LDA-based tight-binding simulations a first peak at 3.8 eV and second peak at 5.9 eV. Gupta *et al.*[25] found (with an LDA-based FLAPW method) all the experimental features, but with a shift of at least 1 eV toward lower energies for the tetragonal phase and of more than 1 eV for the cubic phase. Bagayoko *et al.*[19] calculated the optical spectrum of tetragonal BT with a self-consistent LCAO method. The calculated spectrum is in fair agreement with the experiment concerning the main peak (although it appears to be a very sharp double peak at around 4 eV); however, all the features spread over 13 eV in the experimental spectrum appear compressed within 0 to 8 eV.

In Fig. 5 we show the optical spectra calculated for cubic and tetragonal BT within the DFT-GGA and BSE approach. For the tetragonal phase, the complex dielectric constant has been calculated both parallel [$\varepsilon^{\parallel}(\omega)$] and perpendicular [$\varepsilon^{\perp}(\omega)$] to the polarization. The spectrum obtained within DFT-GGA for cubic BT [Fig. 5(a)] agrees roughly with earlier independent-particle results.[19,23,25] There are two main features of the optical absorption centered at about 3.9 eV (P_1) and 8.4 eV (P_2, with smaller shoulder peaks P_2' and P_2'' at 6.8 and 9.6 eV), as indicated by the arrows. The first peak has been attributed to transitions from the lower states of the O 2p valence band to the lower states of the Ti 3d conduction band and from transitions from the upper states of the O 2p valence band to the upper states of the Ti 3d conduction band. The second peak has been attributed to transitions from the lower states of the O2 p valence band to the upper states of the Ti 3d conduction band. The spectrum calculated for tetragonal BT for the x and y directions [$\varepsilon^{\perp}(\omega)$ in Fig. 5(b)] does not differ substantially from the spectrum of cubic BT. $\varepsilon^{\parallel}(\omega)$ shows peaks shifted toward higher energies instead [Fig. 5(c)]. The positions of P_1 and P_2 are shifted by almost 1 and 2 eV, respectively, toward lower energies compared to experiment, because of the inadequate DFT-GGA description of the band gap and excited states. In agreement with Gupta *et al.*, we observe that even if the band structures of cubic and tetragonal BT are very similar, the optical properties are rather sensitive to the tetragonal distortion.

The Coulomb correlation of electrons and holes, accounted for by solving the BSE, improves the theoretical description substantially. This concerns both the peak positions and the line shapes, which sharpen because of the inclusion of excitonic effects. P_1 becomes more pronounced and the whole feature is blueshifted compared to the DFT-GGA spectrum. Concerning cubic BT, the main peak is positioned at about 4.9 eV, while the second peak is now shifted to the experimental value around 10 eV. A similar behavior is observed in tetragonal BT for $\varepsilon^{\perp}(\omega)$, while $\varepsilon^{\parallel}(\omega)$ shows a different spectrum, in which all the previously discussed peaks can be identified, but with a different reciprocal height than in $\varepsilon^{\perp}(\omega)$ [see Fig. 5(c)].

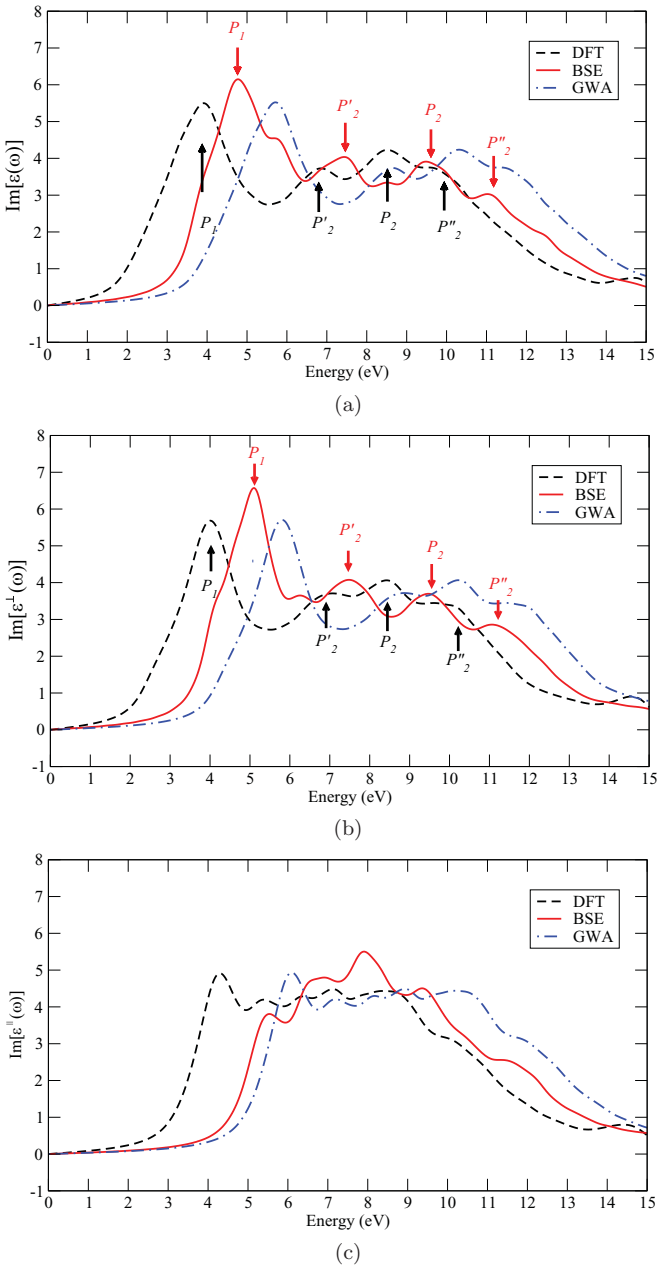

FIG. 5. (Color online) Complex dielectric function of cubic (a) and tetragonal [(b) and (c)] BT calculated within the DFT-GGA and GWA and from the BSE.

Comparing the calculated GWA and BSE spectra, we find the onset of the optical absorption to be modified by about 0.5 eV for the cubic phase and by about 0.5 and 0.3 eV [$\varepsilon^{\parallel}(\omega)$ and $\varepsilon^{\perp}(\omega)$] for the tetragonal phase. This is close to the difference between the GWA band gap of 3.7 eV and the experimental measured value of 3.3 eV for the cubic phase. Optical excitations at higher energies, such as the P_2 peak, experience even larger excitonic effects, of the order of 1 eV. Our BSE calculations represent the best agreement of a first-principles theoretical model with the experimental results so far. We mention that our GW and BSE calculations do not contain the contribution of the lattice polarizability to the dressing of the quasiparticles. It may be expected that

this contribution is important in polar materials such as BT that feature longitudinal optical phonons that give rise to macroscopic electric fields that couple to the excited electrons and holes and modify their motion.[68]

IV. THE TETRAGONAL-CUBIC PHASE TRANSITION

We have calculated the Curie temperature ϑ_c of BT by evaluating the free energies of the tetragonal and cubic phases as described in Sec. II. We thereby do not restrict our calculation to the Γ modes of Table III, but consider the phonon frequencies at other high-symmetry points of the Brillouin zone too. These are obtained using a supercell that is $2 \times 2 \times 2$ the BT primitive cell. In this way, the vibrations at all the high-symmetry points listed in Fig. 4 are considered. The parameters of our calculation correspond to the values mentioned in Sec. III B

We predict that the tetragonal-cubic phase transition will occur at around 419 K. At this temperature the contribution of the vibrational entropy is large enough to compensate for the lower total energy of the tetragonal phase at $T = 0$ (see Fig. 6). The discrepancy between the calculated and measured value is about 25 K. This difference can be explained by different sources of error that we discuss in the following. They are either due to intrinsic limitations of our model (i.e., approximations in our thermodynamics approach and anharmonic effects not considered in our calculation) or are of numerical nature (i.e., the finite sampling of the phonon modes in the Brillouin zone and the precision of the calculations itself).

As discussed in Sec. II, our estimation of the transition temperature is based on the evaluation of the free energy $F = F(V,T) = U(S,V) - TS$ of the two phases. We thereby approximate the internal energy $U = U(S,V)$ by the DFT total energy $E(V_0)$, calculated for $V_0 = V_{T=0}$, i.e., neglecting the effect of the temperature on the volume and on the entropy as well. If the considered volume strongly depends on the temperature, this approximation becomes less accurate at higher temperatures. In our case, however, this approximation is justified by the thermal behavior of BT. Similarly to other distortion ferroelectrics, the volume of the material grows with the temperature to a certain value, and decreases again close to the Curie temperature ϑ_c. Using the linear coefficient of thermal expansion reported in Ref. 69 for $T \approx T_c$ ($\alpha = -1.2 \times 10^{-6}$ K^{-1}), we repeat our calculations at $V_c = V_{T=\vartheta_c}$. This leads to an increase of the free energy of the two phases by less than 1 meV and therefore to no change in the calculated transition temperature. The approximation of $U = U(S,V)$ with the DFT total energy $E(V_0)$ cannot therefore be the reason for the deviation from the measured value.

Another crucial point is the sampling of the phonon dispersion relations. As pointed out by Xie *et al.*[22] the phonon modes of BT show a pronounced dispersion within the Brillouin zone. An accurate sampling of the latter is therefore necessary to have a complete picture of the vibrational frequencies. In this work, we have considered phonon modes calculated at all the high-symmetry points of the Brillouin zone represented in Fig. 4, namely Γ, X, M, and R for the cubic phase and Γ, X, M, R, Z, and A for the tetragonal phase. To estimate the error due to the finite sampling, we have restricted step by step the

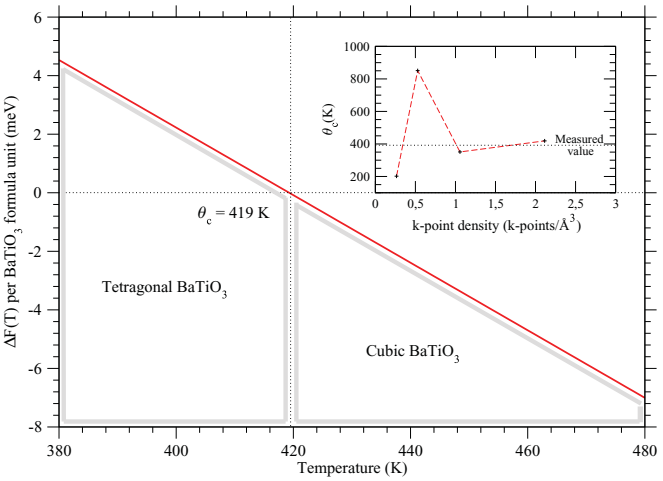

FIG. 6. (Color online) Calculated free energy difference between the cubic and tetragonal phases as a function of the temperature. Transition temperature and stable phase are indicated. The inset shows the calculated transition temperature as a function of the phonon sampling.

number of k points and calculated the transition temperature again. The results of this procedure are plotted in the inset of Fig. 6. Considering merely the frequencies of the Γ-point modes, the transition temperature rises to 863 K, indicating that a Γ-point sampling is not sufficient for a reasonable estimate of the transition temperature. Extending the sampling of the phonon dispersion leads to a better agreement with the measured value, until a converged value is reached by taking into account the phonon modes at all high-symmetry points of the Brillouin zone. Strictly speaking only an ideal sampling (i.e., as obtained using an infinitely large BT supercell) would lead to an exact evaluation of the frequencies, and each finite sampling will introduce some error. However, our choice of the k points seems to be exhaustive enough to reduce this error to no more than 10–15 K.

The frequencies of the longitudinal modes, which are affected by long-range polarization effects, are not accurately reproduced within our approach. Although this problem concerns both the cubic and the tetragonal phases and will therefore be of the same extent subject to error cancellation, it will nevertheless contribute to the deviation between calculated and measured phase transition temperatures. So will anharmonicity effects, which are certainly not negligible at $T = \vartheta_c$. If the lattice dynamics can be described by (small) harmonic vibrations around the total energy minimum, Eq. (5) gives the vibrational contribution to the free energy. A few modes belonging to TO1 represent a saddle point of the total energy, though (see Sec. III B). These vibrations are included in our calculation and treated as harmonic modes; therefore Eq. (5) only holds in approximate form. The uncertainty in the temperature estimation due to the accuracy of the total energy calculations is low. It amounts to about 1 K if we assume an energy deviation of 0.1 meV.

An upper bound of the numerical error of our model due to the precision of the calculation is obtained by modifying the calculated phonon frequencies entering Eq. (5) by an amount equal to the deviation from the measured values. As

the phonon frequencies are varied, the transition temperature ranges within an interval of 100 K, which is then supposed to be the uncertainty of our model. Within this margin, the calculated transition temperature is in agreement with the measured value. Our calculations clearly confirm that the gain in vibrational entropy of the cubic phase at high temperatures compensates for the structural energy difference with the tetragonal phase. An analysis of the entropic contributions of the single-phonon branches reveals that the gain in vibrational entropy is roughly equally divided between the phonons and cannot be traced back to a single mode.

V. SUMMARY

We have performed first-principles calculations of the structural, vibrational, electronic, and optical properties of $BaTiO_3$. The ground-state structures and phonon frequencies calculated in the present work agree well with experiment and earlier *ab initio* calculations. While the DFT-GGA underestimates the electronic band gap, quasiparticle effects widen the band gap by 2 eV in both investigated phases. On the other hand, strong excitonic effects with exciton binding energies up to 1 eV are predicted. The ferroelectric phase transition has been investigated by *ab initio* thermodynamics. This approach gives a reasonable estimate of the phase transition temperature, calculated at 419 K.

ACKNOWLEDGMENTS

The calculations were done using grants of computer time from the Paderborn Center for Parallel Computing (PC^2) and the Höchstleistungs-Rechenzentrum Stuttgart (HLRS). The Deutsche Forschungsgemeinschaft is acknowledged for financial support.

*simone.sanna@uni-paderborn.de

[1] H. T. Evans, Acta Crystallogr. **4**, 377 (1951).
[2] G. Shirane, H. Danner, and R. Pepinsky, Phys. Rev. **105**, 856 (1957).
[3] P. Ghosez, X. Gonze, and J.-P. Michenaud, Ferroelectrics **220**, 1 (1999).
[4] P. Voudsen, Acta Crystallogr. **9**, 141 (1955).
[5] M. Yamaguchi, K. Inoue, T. Yagi, and Y. Akishige, Phys. Rev. Lett. **74**, 2126 (1995).
[6] R. Waser, *Nanoelectronics and Information Technology: Advanced Electronic Materials and Novel Devices* (Wiley-VCH, Weinheim, 2003).
[7] F. Jona and G. Shirane, *Ferroelectric Crystals* (Macmillan, New York, 1962).
[8] G. H. Kwei, A. C. Lawson, S. J. L. Billinge, and S. W. Cheong, J. Phys. Chem. **97**, 2368 (1993).
[9] S. H. Wemple, Phys. Rev. B **2**, 2679 (1970).
[10] M. Cardona, Phys. Rev. **140**, A651 (1965).
[11] D. Bäuerle, W. Braun, V. Saile, G. Sprüssel, and E. E. Koch, Z. Phys. B **29**, 179 (1978).
[12] W. Spitzer, R. Miller, D. Kleinman, and L. Howarth, Phys. Rev. **126**, 1710 (1962).
[13] Y. Luspin, J. Servoin, and F. Gervais, J. Phys. C **13**, 3761 (1980).
[14] R. Scharfschwerdt, A. Mazur, O. F. Schirmer, H. Hesse, and S. Mendricks, Phys. Rev. B **54**, 15284 (1996).
[15] S. Schlag and H.-F. Eicke, Solid State Commun. **91**, 883 (1994).
[16] F. M. Michel-Calendini and G. Mesnard, Phys. Status Solidi B **44**, K117 (1971).
[17] F. M. Michel-Calendini and G. Mesnard, J. Phys. C **6**, 1709 (1973).
[18] R. E. Cohen and H. Krakauer, Phys Rev B **42**, 6416 (1990).
[19] D. Bagayoko, G. Zhao, J. Fan, and J. Wang, J. Phys. Condens. Matter **10**, 5645 (1998).
[20] R. Khenata, M. Sahnoun, H. Baltache, M. Rerat, A. H. Rasheck, N. Illes, and B. Bouhafs, Solid State Commun. **136**, 120 (2005).
[21] R. King-Smith and D. Vanderbilt, Ferroelectrics **136**, 85 (1992).
[22] Y. Xie, H. Yu, G. Zhang, and H. Fu, J. Phys. Condens. Matter **20**, 215215 (2008).
[23] S. Saha, T. P. Sinha, and A. Mookerjee, Phys. Rev. B **62**, 8828 (2000).
[24] K. Saha, T. Saha-Dasgupta, A. Mookerjee, S. Saha, and T. P. Sinha, J. Phys. Condens. Matter **14**, 3849 (2002).
[25] G. Gupta, T. Nautiyal, and S. Auluck, Phys. Rev. B **69**, 052101 (2004).
[26] C. B. Samantaray, H. Sim, and H. Hwang, Microelectron. J. **36**, 725 (2005).
[27] P. Hohenberg and W. Kohn, Phys. Rev. **136**, B864 (1964).
[28] W. Kohn and L. J. Sham, Phys. Rev. **140**, A1133 (1965).
[29] S. E. Tinte, M. G. Stachiotti, C. O. Rodriguez, D. L. Novikov, and N. E. Christensen, Phys. Rev. B **58**, 11959 (1998).
[30] P. Goudochnikov and A. Bell, J. Phys. Condens. Matter **19**, 176201 (2007).
[31] D. I. Bilc, R. Orlando, R. Shaltaf, G.-M. Rignanese, J. Íñiguez, and P. Ghosez, Phys. Rev. B **77**, 165107 (2008).
[32] R. Wahl, D. Vogtenhuber, and G. Kresse, Phys. Rev. B **78**, 104116 (2008).
[33] D. M. Ceperley and B. J. Alder, Phys. Rev. Lett. **45**, 566 (1980).
[34] J. P. Perdew, K. Burke, and M. Ernzerhof, Phys. Rev. Lett. **77**, 3865 (1996).
[35] A. D. Becke, J. Chem. Phys. **98**, 5648 (1993).
[36] R. Dovesi, R. Orlando, B. Civalleri, C. Roetti, V. R. Saunders, and C. M. Zicovich-Wilson, Z. Kristallogr. **220**, 571 (2005).
[37] A. D. Becke, J. Chem. Phys. **104**, 1040 (1996).
[38] J. P. Perdew and Y. Wang, Phys. Rev. B **33**, 8800 (1986).
[39] M. S. Hybertsen and S. G. Louie, Phys. Rev. B **34**, 5390 (1986).
[40] S. Albrecht, L. Reining, R. Del Sole, and G. Onida, Phys. Rev. Lett. **80**, 4510 (1998).
[41] L. X. Benedict, E. L. Shirley, and R. B. Bohn, Phys. Rev. Lett. **80**, 4514 (1998).
[42] M. Rohlfing and S. G. Louie, Phys. Rev. Lett. **83**, 856 (1999).
[43] L. J. Sham and T. M. Rice, Phys. Rev. **144**, 708 (1966).
[44] W. Hanke and L. J. Sham, Phys. Rev. B **12**, 4501 (1975).
[45] W. Hanke and L. J. Sham, Phys. Rev. B **21**, 4656 (1980).
[46] P. E. Blöchl, Phys. Rev. B **50**, 17953 (1994).
[47] G. Kresse and J. Furthmüller, Phys. Rev. B **54**, 11169 (1996).
[48] J. P. Perdew, J. A. Chevary, S. H. Vosko, K. A. Jackson, M. R. Pederson, D. J. Singh, and C. Fiolhais, Phys. Rev. B **46**, 6671 (1992).

[49]R. D. King-Smith and D. Vanderbilt, Phys. Rev. B **49**, 5828 (1994).
[50]H. J. Monkhorst and J. D. Pack, Phys. Rev. B **13**, 5188 (1976).
[51]F. Bechstedt, R. Del Sole, G. Cappellini, and L. Reining, Solid State Commun. **84**, 765 (1992).
[52]W. G. Schmidt, S. Glutsch, P. H. Hahn, and F. Bechstedt, Phys. Rev. B **67**, 085307 (2003).
[53]P. H. Hahn, W. G. Schmidt, and F. Bechstedt, Phys. Rev. Lett. **88**, 016402 (2001).
[54]S. Wippermann and W. G. Schmidt, Phys. Rev. Lett. **105**, 126102 (2010).
[55]S. Sanna and W. G. Schmidt, Phys. Rev. B **81**, 214116 (2010).
[56]*Ferroelectrics and Related Substances*, edited by K. H. Hellwege and A. M. Hellwege, Landolt-Börnstein, New Series, Group III, Vol. 3 (Springer Verlag, Berlin, 1969).
[57]M. Gajdoš, K. Hummer, G. Kresse, J. Furthmüller, and F. Bechstedt, Phys. Rev. B **73**, 045112 (2006).
[58]S. Baroni and R. Resta, Phys. Rev. B **33**, 7017 (1986).
[59]X. Wu, D. Vanderbilt, and D. R. Hamann, Phys. Rev. B **72**, 035105 (2005).
[60]F. Bernardini, V. Fiorentini, and D. Vanderbilt, Phys. Rev. B **56**, R10024 (1997).
[61]M. Zgonik, P. Bernasconi, M. Duelli, R. Schlesser, P. Günter, M. H. Garrett, D. Rytz, Y. Zhu, and X. Wu, Phys. Rev. B **50**, 5941 (1994).
[62]Z. Li, S.-K. Chan, M. H. Grimsditch, and E. S. Zouboulis, J. Appl. Phys. **70**, 7327 (1991).
[63]X. Meng, X. Wen, and G. Qin, Comput. Mater. Sci. **49**, S372 (2010).
[64]H. Siethoff and K. Ahlborn, J. Appl. Phys. **79**, 2968 (1995).
[65]D. L. Decker and Y. X. Zhao, Phys. Rev. B **39**, 2432 (1989).
[66]W. G. Schmidt, F. Bechstedt, and G. P. Srivastava, Phys. Rev. B **52**, 2001 (1995).
[67]L. T. Hudson, R. L. Kurtz, S. W. Robey, D. Temple, and R. L. Stockbauer, Phys. Rev. B **47**, 1174 (1993).
[68]F. Bechstedt, K. Seino, P. H. Hahn, and W. G. Schmidt, Phys. Rev. B **72**, 245114 (2005).
[69]Y. He, Termochim. Acta **419**, 135 (2004).